

A platform for trapped cryogenic electrons, anions and cations for fundamental physics and chemical studies

L. O. A. Azevedo¹, R. J. S. Costa¹, W. Wolff¹, A. N. Oliveira², R.L. Sacramento¹, D.M. Silveira¹, C. L. Cesar^{1*}

¹Instituto de Física, Universidade Federal do Rio de Janeiro, Rio de Janeiro 21941–909, Brazil

²INMETRO, Caxias, 219999, Brazil

Abstract:

Cryogenic cations, electrons and anions are ubiquitous in space, participate on star formation chemistry and are relevant to studies on the origin of molecular biology homochirality. We report on a system to directly generate and trap these species in the laboratory. Laser ablation of a solid target (LiH) facing a sublimating Ne matrix generates cryogenic electrons, anions, and cations. Axial energy distributions (of e^- , H^\pm and Li^\pm) peaked at 0–25 meV are obtained in a Penning trap at 90 mT and 0.5 eV barrier. Anions can be guided and turned neutral with low recoil energy by near-threshold photodetachment. An immediate prospect for this H^- source is to load hydrogen atoms into the ALPHA antihydrogen trap at CERN towards direct spectroscopic comparison of both conjugated species beyond 13 significant figures. The production is scalable and adaptable to different species including deuterium and tritium, relevant for neutrino mass and fusion research.

Introduction

Sources and traps of cold negative and positive species are needed to study the low-temperature species themselves and the reactions between trapped charged particles and neutral species¹. Crucial requirements on both, sources and traps, represent a significant challenge due to specific limitations and conditions on a variety of setups. Here, we report source and trap with innovative methods with an integrated mass discriminator, describing the elements and quantitatively assessing their performance. Many of the innovations and findings are of general interest, as briefly presented for diverse applications.

Measurements of the 1S–2S transition frequency in antihydrogen (\bar{H}) by the ALPHA collaboration at 12 significant figures^{2,3} entered uncharted territory in the comparison of charge conjugated species, a test of the Charge–Parity–Time (CPT) symmetry. We foresee the need to perform laser spectroscopy of H in the same trap⁴ as \bar{H} to achieve aimed precisions of 15 significant figures in search of explanations for the matter–antimatter asymmetry in the Universe. In the same trap and reference frame, both species could be studied under the same conditions enabling better control over systematic effects, such as trap magnetic fields and laser power causing AC Stark shift –. The \bar{H} research program also involves probing the gravitational acceleration^{5,6}. Antihydrogen is produced – from its constituents, antiproton and positron – and studied in challenging conditions, such as an exquisite ultra-high-vacuum (UHV) environment to avoid annihilation to background gas.

Thus, it is not always possible to readily use normal matter techniques to load the antimatter trap with matter species. For example, H has been trapped and subjected to high-precision laser spectroscopy at MIT⁷ and Amsterdam⁸ in a trap that required a superfluid liquid helium covered cell, conditions incompatible with the $\bar{\text{H}}$ trap at CERN. Therefore, innovative techniques are required for loading H in the $\bar{\text{H}}$ trap and the developments presented here can be readily adapted as a solution.

The samples of H^- produced by our system are within the temperature of the antiproton and positron samples used by the ALPHA experiment for $\bar{\text{H}}$ synthesis. The H^- can be produced and trapped adjacent to the main apparatus, and after the UHV condition is regained, the anions will be guided into the composed, Penning and magnetic, ALPHA trap. They can be further cooled by evaporative cooling by themselves or with pre-cooled electrons. Then, a laser pulse, with photon energy near the photodetachment threshold⁹ of H^- (0.754 eV), will neutralize the anions imparting low recoil energy. For example, a laser at 1575 nm will leave 0.2 K of recoil energy – less than the typical temperature or energy dispersion of the ion sample – to the neutral H. The fraction of resulting atoms with energy below 0.5 K will remain trapped in the superposed magnetic trap.

Moreover, the developments with $\bar{\text{H}}$ research have spurred a renewed interest in hydrogen trapping and spectroscopy by many groups. New techniques to produce cold hydrogen¹⁰⁻¹³ are being investigated with interests ranging from wavefunction in gravity quantum reflection¹⁴, to scientific metrology – in tests of Quantum Electrodynamics, proton radius puzzle, and search for variation of fundamental constants – and to produce larger Bose-Einstein condensates. The system presented offers an alternative, study model, or a proof-of-principle for some of these studies. For example, the generation of cold H from H^- is the charge conjugated process from one proposed experiment^{15,16} for measuring gravity with $\bar{\text{H}}$.

The present demonstration, starting from laser ablation of LiH and generating H^- , Li^- and Li_nH_m^- does not show, a priori, a specificity that would prevent it from being applicable to other simple species, such as D^- and T^- . An example of such a specificity is the case of the MIT and Amsterdam H traps that could not trap¹⁷ D because of its slightly higher binding energy to liquid helium. A proposal for neutrino mass measurement^{18,19} requires quasi-trapped tritium for the experiment to be performed in a magnetic field. Many low-energy atomic processes involving deuterium are relevant in fusion research²⁰ for a copious production of D^- . The source here described, adapted for T^- and D^- , might find use for these studies.

Lastly, the interaction of low energy ions and electrons with neutral atoms and molecules is important from astrophysics to the origin of biological molecules²¹⁻²³. It would thus be desirable to have a platform to generate various cryogenic species in a direct way. Producing

and trapping slow anions is not trivial. Stray or contact electric fields can easily generate thousands of kelvins, since an energy of only 26 meV is equivalent to 300 K in temperature scale. Difference of work functions in metals can reach 1 V. Patch or domain potentials within an electrode²⁴ can reach 250 mV. Anions are typically created at energies²⁵ of many eV or keV. Various methods have been employed for further cooling ionized species: – entrainment in buffer gas^{26,27}; – resistive cooling²⁸; – direct sympathetically cooling²⁹ and LC mediated sympathetic cooling³⁰; – direct laser cooling for species, such as cations³¹ and proposed for molecular anions³², with nearly closed optical transitions.

At the ALPHA experiment, where the \bar{H} trapping rate depends strongly on a low positron cloud temperature, the final cooling to ~ 20 K relies on evaporative cooling³³. In summary, there are many different techniques being explored and developed to produce cold charged samples due to their scientific relevance. Here, we report on a platform to directly generate: (i) electrons with a perspective for a cryogenic polarized electron beam; (ii) simple molecular ions at temperatures compatible with interstellar media chemistry; (iii) hydrogen anions suitable for antihydrogen research in a method adaptable to deuterium and tritium research. It may also serve as an attractive initial step towards samples in the cold and ultracold regime.

Experimental Setup and Procedures

The method is based on the Matrix Isolation Sublimation (MISu) technique^{34–37} and variations. In MISu, beams of atoms and molecules can be produced either in a fast pulse (in ~ 10 – 100 μ s) or in a quasi-continuous beam depending on the sublimation regime. The implantation of different atoms into the rare-gas matrix, typically via laser ablation of solid precursor such as pellets of LiH, Ca, Cr, graphite, can lead to the formation of molecules within the matrix. As previously reported³⁷, we produced Li_nCa_m molecules from alternating laser ablation of a Li and a Ca pellet. Since electrons should not attach to the Ne atoms, it was initially thought that implanting electrons together with atoms and molecules would lead to the formation of different anionic species in the matrix. As a faster variation, we found that the laser ablated species impinging onto the Ne matrix already generate low-energy electrons and atomic or molecular ions.

The sapphire substrate, upon which we deposit the neon matrix, is coated on both sides with NiCr resistive film. The back film is used as a resistor to apply a sublimating heat pulse while the front film serves as a mirror and provides a way to bias the sapphire with a positive or negative voltage. This bias can be used to repel or attract the species to the matrix during the ablation process and/or during the sublimation phase.

In figure 1 we present the basic setup used in this study. A two-stage closed cycle cryostat with 1 W of cooling power at 4 K is used. An UHV environment can be achieved below 6.9 K, where the saturated vapor pressure of Ne is predicted to be $\sim 7.5 \times 10^{-10}$ Torr and falls 12 orders of magnitude at 4 K if one had a vacuum tight enclosure. This UHV condition is not met during the matrix growth or sublimation, and it takes milliseconds for the Ne gas to cryopump back to the walls. Due to a poor thermal link in the present setup, the trap electrodes region only reaches ~ 6.5 K while the main chamber is at ~ 4 K. The sapphire substrate is thermally anchored to the “4K plate” through a designed thermal link that allows it to reach 3.2 K and be heated for the sublimation process without warming the whole experimental cell. The Ne gas delivery tube is brought into the cryostat with a first thermal link at the 1st stage (40 K nominal) and its exit is above 16 K, to avoid plugging, and directed towards the sapphire. The laser reflections on the interfaces, vacuum–matrix and matrix–sapphire, cause interference fringes that allow monitoring the matrix thickness down to the atomic monolayer as well as performing Doppler-sensitive spectroscopy of neutral Li atoms as they sublime from the matrix into vacuum.

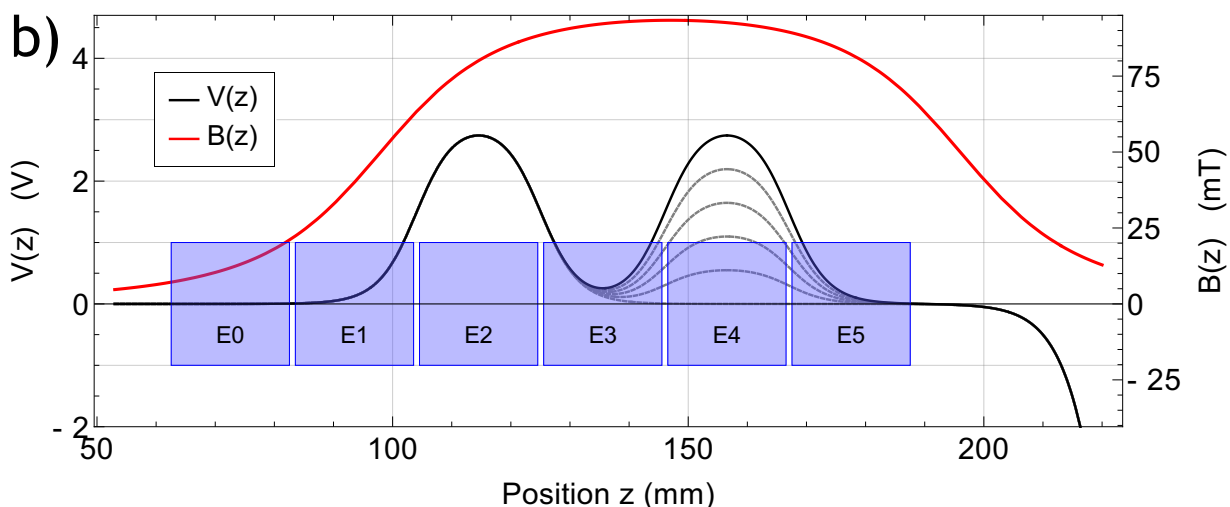
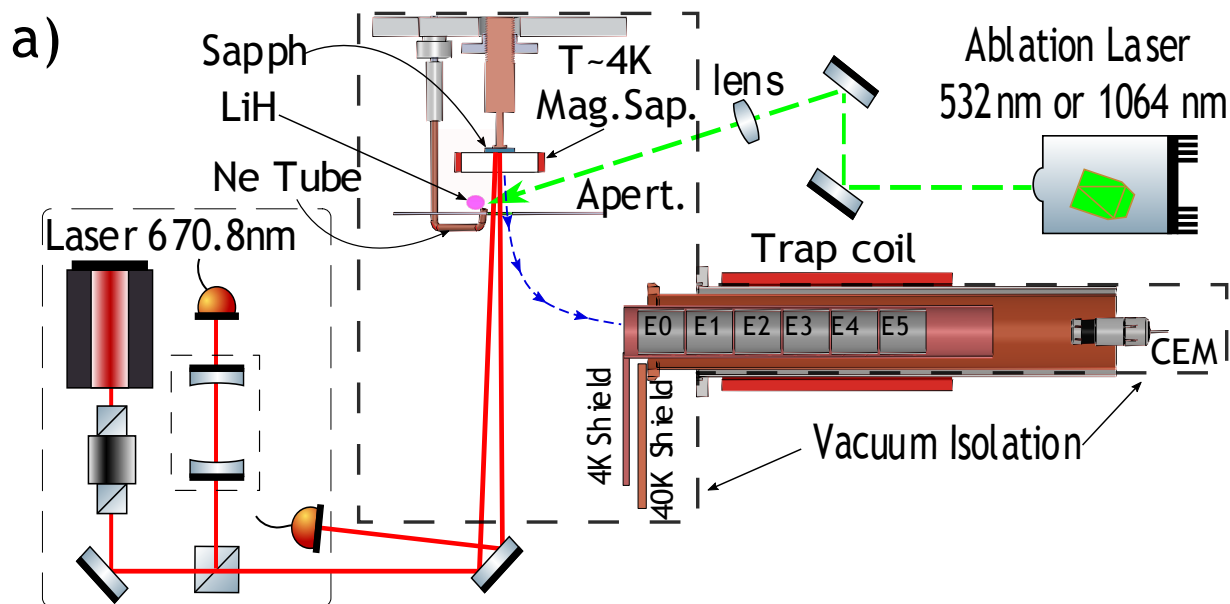


Figure 1. a) A diagram of the basic setup is shown. The sapphire (“Sapph”) where the Ne matrix is deposited, as the gas is delivered through the tube, and the inner chamber are thermally anchored at the 2nd stage 4 K cryohead surrounded by a “40K” black-body shield. The spectroscopy laser monitors the matrix thickness and the Li atoms absorption. A pulsed laser at 532 or 1064 nm (in dashed green) promotes ablation from a LiH pellet imparting atoms, molecules, electrons, and ions onto the Ne matrix. Two magnets, “Mag.Sap.” and “Trap coil”, for guiding (dotted blue arrows) and trapping are placed around the sapphire and the trap region. An aperture avoids excess Ne gas towards the cell bottom and trap region. The Penning–Malmberg trap uses six ring electrodes (E0–E5), glued externally to a grounded copper tube that reaches 6.5 K, and is followed by a channeltron CEM detector. The CEM is loosely thermally anchored to the “40K” stage. b) Axial profiles of the magnetic field (red line) and a configuration, for cations, of the potentials for a dump at E4 (black solid line going in time to the lowered dotted curves) for a trap initially centered around E3.

During or after the matrix growth a single, or multiple, laser ablation pulses onto the appropriate solid precursor – mainly LiH during this study – release and implant neutral and

charged particles into the matrix or reflect from it. The matrix can be sublimated at different times with respect to the ablation pulses. We have employed many variations on these timing parameters and laser pulse energies. For ablation we mostly employed a doubled Nd:YAG at 532 nm, with a few mJ in 5 ns pulses. This flashlamp pumped laser became unreliable and we switched to a diode laser pumped Nd:YAG at 1064 nm with up to 1.5 mJ using a tighter focusing for similar fluences. The front sapphire terminal can be monitored for the charge deposited into (or released from) the matrix, acting as a capacitor, during the ablation (or sublimation) process. Through laser ablation, enough charge can be deposited to achieve many volts of space charge or to thermally explode the matrix. Both the ablation process and space charge variations can affect the results. We monitored the matrix size, the deposited charge, and the sapphire temperature change due to the ablation and sublimation. Adjusting these parameters and the very critical timing for switching the trapping electrodes potentials, we have conducted hundreds of experimental cycles in a robust manner.

A dry superconducting coil ("Mag. Sap." in Fig. 1) placed around the sapphire generates a field of ~ 41 mT in a configuration to guide the particles into the trap region. The Penning-Malmberg trap, in the horizontal direction, is composed of six similar electrodes, named E0–E5, of 17.4 mm of inner diameter and 20 mm length each. The magnetic field at the trap is generated by an external resistive coil ("Trap coil" in Fig. 1) which produces 92 mT on axis, around E3–E4, at 100 A. Such a short coil was dictated by space constraints and resulted in a highly non-uniform field. This leads to magnetic mirroring reflections if we dump the particles from electrodes E2–E3. Due to heating, the coil can only be left energized for ~ 1.5 second, limiting the trapping time. The resulting field from the two coils generates a guiding magnetic field that leads the particles from the source making a turn into the trap. Along the guiding lines, the field reach values as low as 1.5 mT, which is enough for guiding low energy and low mass species.

For detection of the charged species, we use a Channel Electron Multiplier (CEM), a Magnum Channeltron from Photonis Inc, to the right of electrode E5 in Fig.1. We set the voltages in the CEM to attract either negative or positive charges before each experiment. For cations, the cone of the CEM is set at -2 kV while the anode is grounded via a load resistor of 1 k Ω . For anions, the cone is set at +0.4 kV while the anode is connected to +2.4 kV via a 1.2 M Ω resistor. In both configurations the output is capacitively coupled out of the cryostat and into a radio-frequency pre-amplifier which is directly recorded by an oscilloscope at 40 GSa/s, with up to 5 ms acquisition, and analysed by a peak detection routine above a certain threshold. To prevent excess black-body heat coming from the CEM into the trap we partially anchor the wires to the CEM at the 40 K heat shield, at the known expense of a higher detector's resistance resulting in longer recharging times. With a high detection rate, we had to deal with saturation of the cold detector. Particularly, using a fast dump configuration for

a time-of-flight mass discrimination (ToF) for negative particles, the first coming electron signal can saturate the CEM that ends up detecting very few H^- afterwards.

Experimental Results

Initial experiments involved using a homemade time-of-flight mass spectrometer (ToF-MS) to detect the different species emanating from the sapphire (see figure 1). The details of this ToF-MS can be found in ref³⁷. The region where the ions are extracted is large and the ToF-MS resolution is poor, but sufficient to discriminate electrons from H^- and Li^- . A typical mass spectrum of the raw data and histogram is shown in figure 2. The extraction accelerating potential was switched on at 50 μs after ablation. The electrons are detected immediately after the extraction pulse, followed by the heavier species with clear presence of H^- , Li^- and molecular anions. As expected from the ablation of LiH we generated both Li and H ionized species, with both signs of charge, as well as neutral atoms, and molecules.

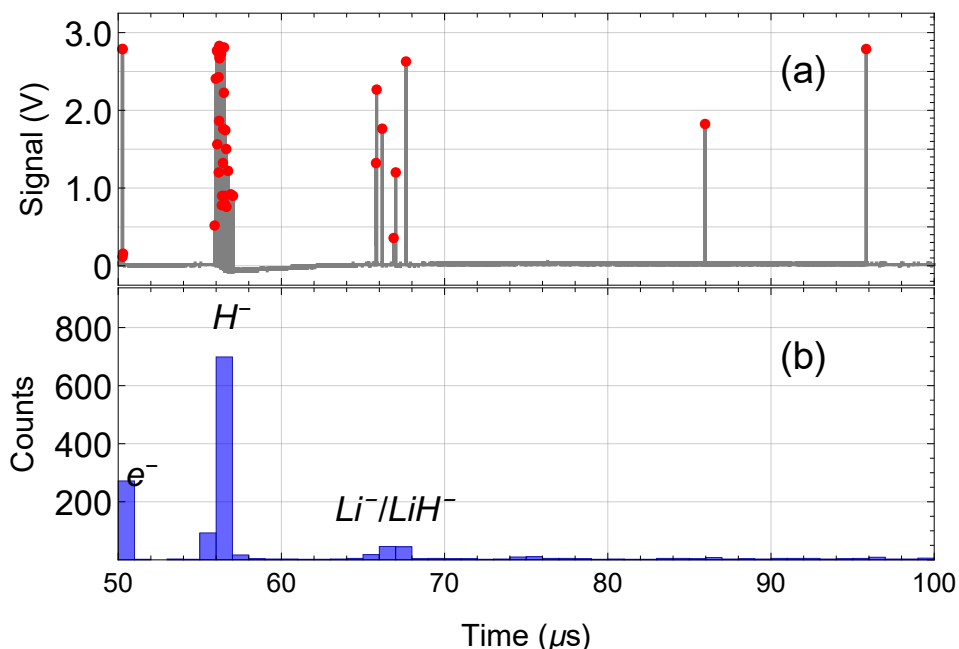


Figure 2. Initial ToF-MS results, in the absence of the trap. The accelerating electric field is switched on at $t=50 \mu s$ after the ablation laser pulse onto the sublimating Ne matrix. The electrons appear immediately, followed by the heavier species. The top graph (a) shows the data collected from the oscilloscope in a single realization. The red dots are peaks identified by the LabView routine. The bottom histogram (b), with mass identification up to Li^- or LiH^- and showing heavier masses, is an accumulation of 35 runs. The fraction of counts for different species depends on timing.

In a MISu procedure the trapping experiment is as follows: (i) the Ne matrix is grown and laser ablation generates and implants atoms, molecules, ions and electrons into the matrix; (ii) both magnets are energized and the Ne matrix is sublimated with a heat pulse starting at time $t=0$, sometimes the last electrode E5 is energized from the beginning; (iii) at time t_1 the entrance trap electrode (E2, for example), or both E2 and E5, is switched on and hold the

trapped ions; (iv) the trapping potentials are manipulated and then lowered at different times and rates and the ions detected in the CEM.

The raw data for cations of a trapping sequence is shown in figure 3. During the slow sublimation (heat pulse starts at $t=0$), the spectroscopy laser (purple trace) continuously scanning (at 2 kHz) around the D2 resonance in Li (670.776 nm) records the atoms' absorption after they are released from the matrix. With $E5 = 5$ V during sublimation, the energy barrier prevents any cation from reaching the CEM. At $t=1080$ μs the entrance electrode E2 is switched, during 20 μs , to 5 V closing the trap. At time $t=3500$ μs the exit electrode E5 is linearly brought, during 800 μs , to 0 V and the ions are detected in the CEM as shown in the blue histogram.

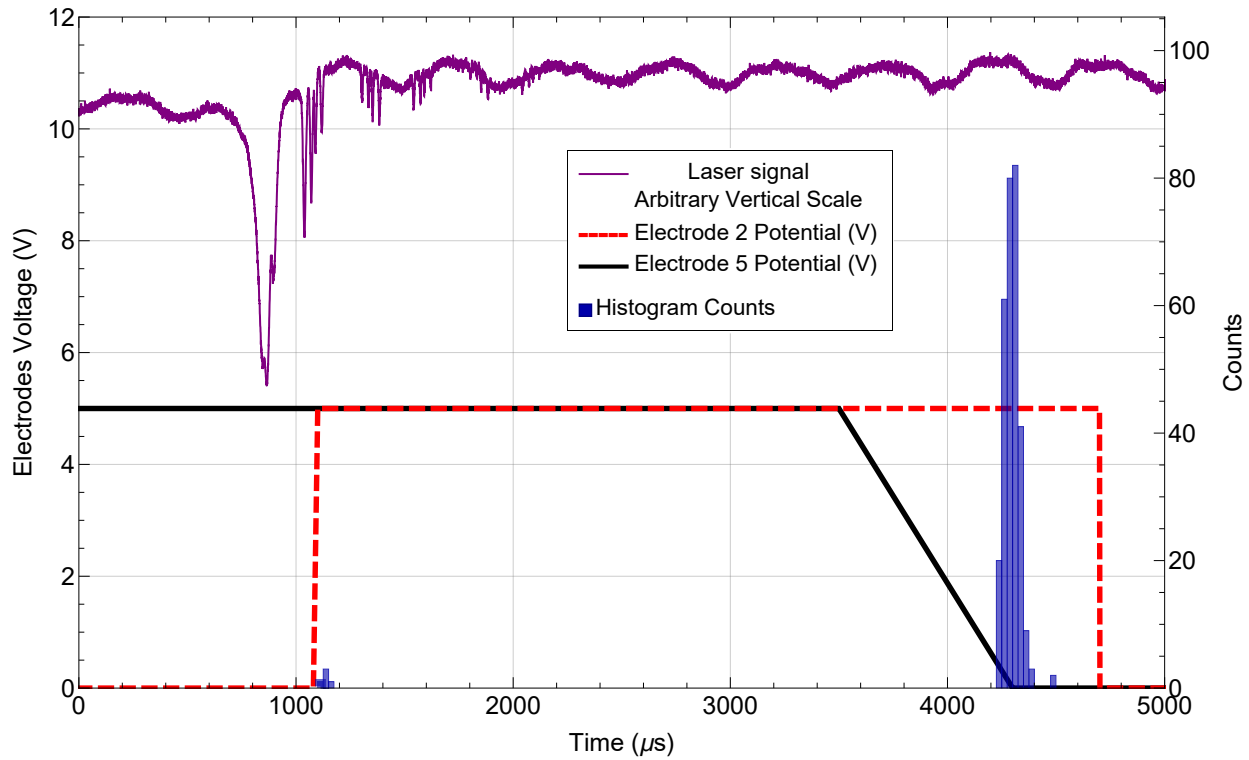


Figure 3. Trapping of cations using the MISu procedure. A matrix is grown while 6 ablation pulses deposit atoms and charged particles into it. At $t=0$, a current is applied to the sapphire's NiCr film resistor causing a slow sublimation of the matrix. The laser transmission is shown in purple and presents information on the matrix thickness and atomic absorption. The E5 electrode (black trace) is set at 5 V since $t=0$. The E2 electrode (red dashed trace) is switched to 5 V at $t=1080$ μs trapping particles between E2 and E5. At $t=3500$ μs , E5 is linearly brought to 0 V and cations are allowed to scape towards the CEM. The cations count is shown in the blue histogram. The appearance of signal at the end of, and after, the ramp is compatible with very low energy ions, despite a small propagation delay of the ions to the detector. The small signal of ions at $t \sim 1100$ μs results from the energy gained by the switching of E2 that pushes ions over the E5 barrier.

Several studies were performed using the MISu procedure described above, with positive and negative charges. The critical optimization parameters include the times between the beginning of the sublimation pulse, the ablation pulse, and the trap closing. Figure 4 shows results for cations done lowering the trap barrier (electrode E4) at a much lower rate than

in figure 3, taking 2500 μs to go from 1 V to 0 V. In this case, the propagation delay to the CEM is of smaller relevance during the ramp down. An energy distribution, incorporating the counts after the ramp down into the first bin, is shown as an inset of the figure. Notice that time and energy are not linear near the end of the ramp as there is a small potential at the central (E3) electrode region. The peak of the distribution is in the first bin (0 to 25 meV) which accounts for 32% of the total counts shown. Among the various manipulations we included squeezing the trap into a single electrode to rid the trap of species with masses higher than 10.

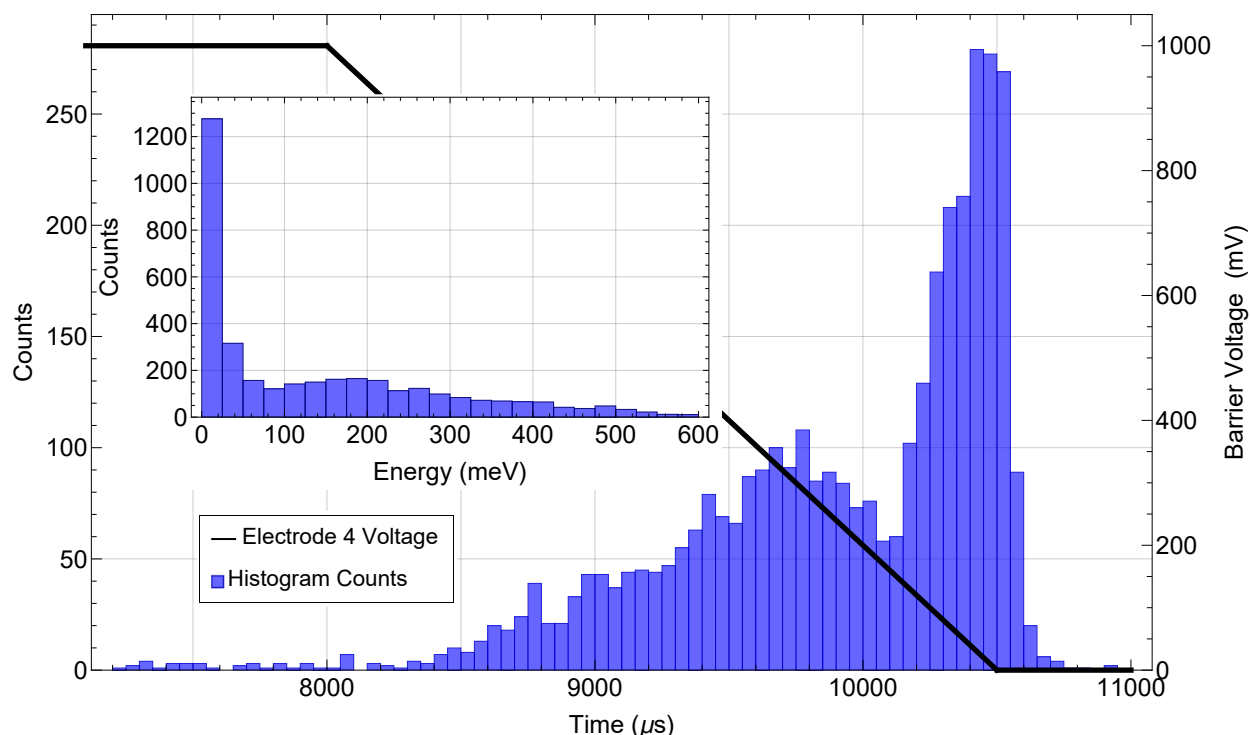


Figure 4. Results with cations (H^+ and Li^+) from the accumulation of 5 runs. A matrix ($\sim 1 \mu\text{m}$) was grown over 20 s with 40 ablation pulses. The sublimation heat pulse started at $t=0$ and the Li atoms were seen (not shown in the graph) sublimating from $\sim 4.5 - 8 \text{ ms}$. An extra ablation pulse is given at $t=6140 \mu\text{s}$ and E2 rose to 5 V from 6200 – 6250 μs closing the trap between E2–E5. The sample was later squeezed between E2–E4 and E4 was brought to 1 V. The histogram (in blue) from the final slow linear dump (from 8000–10500 μs) of E4 from 1 V is shown above in solid black. In the inset the time distribution is mapped into an energy distribution with the counts after the ramp down being incorporated in the first bin (0 – 25 meV).

The result of the studies above with negative charges showed that electrons dominated the counts. To improve the anions' yield, we developed a variation on MISu which consists of applying a single ablation pulse during the sublimation of the Ne matrix. In figure 5, the results of such an experiment for negative charged particles is shown. In this case the trap was manipulated as in figure 4 above, going from an initial trap in E2–E5 to a squeezed E2–E4 and then E4 slowly dumped from -2 V while E2 was kept at -5 V. The time distribution can be folded into an energy distribution shown in the inset with bins of 25 meV.

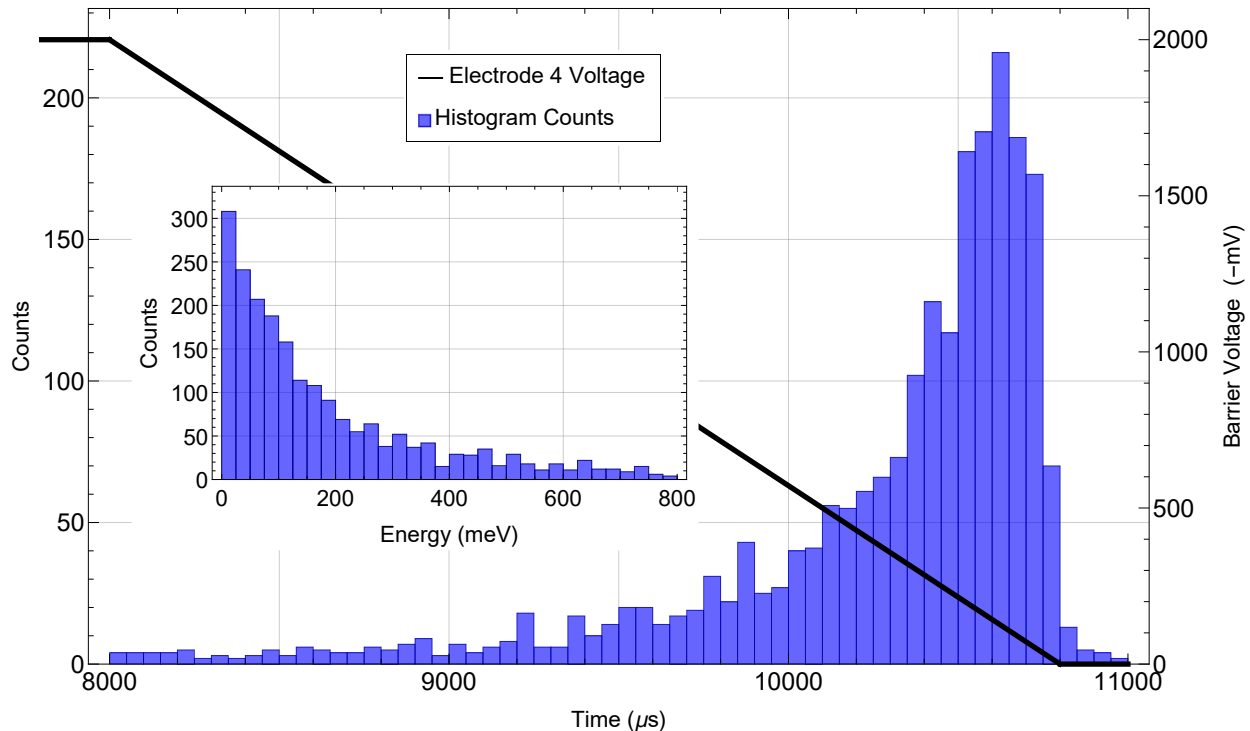


Figure 5. Histogram (in blue) from final dump of electrons and anions (about $1/4$ e^- and $3/4$ H^-) from a trap between E2–E4 after similar manipulations as in figure 4. This data represents the accumulation of 21 runs at a reduced laser energy. The matrix was 80 nm thick. The sublimation heat pulse starts at $t=0$ and a single ablation pulse is given at $t=6140$ μs and E2 rises to -5 V from 6200 – 6250 μs closing the trap between E2–E5. The sample is later squeezed between E2–E4 and E4 is brought to -2 V. The histogram from the final slow linear dump (from 8000–10500 μs) of E4 from -2 V is shown above. The inset shows the corresponding energy distribution, with a nearly exponential decay shape, with the counts after the ramp down being incorporated in the first bin (0 – 25 meV).

To determine which species were trapped, we employed a ToF discrimination in the small space available, far from the ideal Wiley–McLaren³⁸ condition. By trapping the particles in a single electrode, e.g., E2–E4 with E2 at ± 5 V and E4 at ± 1 V, we can quickly lower E4 to ± 0.2 V while raising E3 to ± 0.4 V (where the \pm applies to positive or negative particles) imposing a wiggling acceleration region from E2 to E4 (see Methods for details). The particles are accelerated towards the channeltron and have some short length of free flight. The condition is not ideal but enough to discriminate e^- , H^- and Li^-/LiH^- , though not Li^- from LiH^- . Due to the short length of the trap coil we cannot employ this technique at electrodes farther from the detector. The result of this ToF discriminator is shown in figure 6, using the same matrix and ablation conditions as in figure 5. The ToF discrimination shows electrons and hydrogen anions as majority, followed by a small fraction of Li^- or LiH^- for those conditions. For this procedure we had to considerably decrease the ablation laser energy to avoid saturating the detector with the e^- signal. Details on the simulation are presented in Methods but it is relevant to mention that it is a simple 1D simulation along the axis; that it does not consider the large finite time for the “quick ramp down”, which typically has a 1.2 μs time decay; and that it uses an energy distribution that would reproduce figure 5.

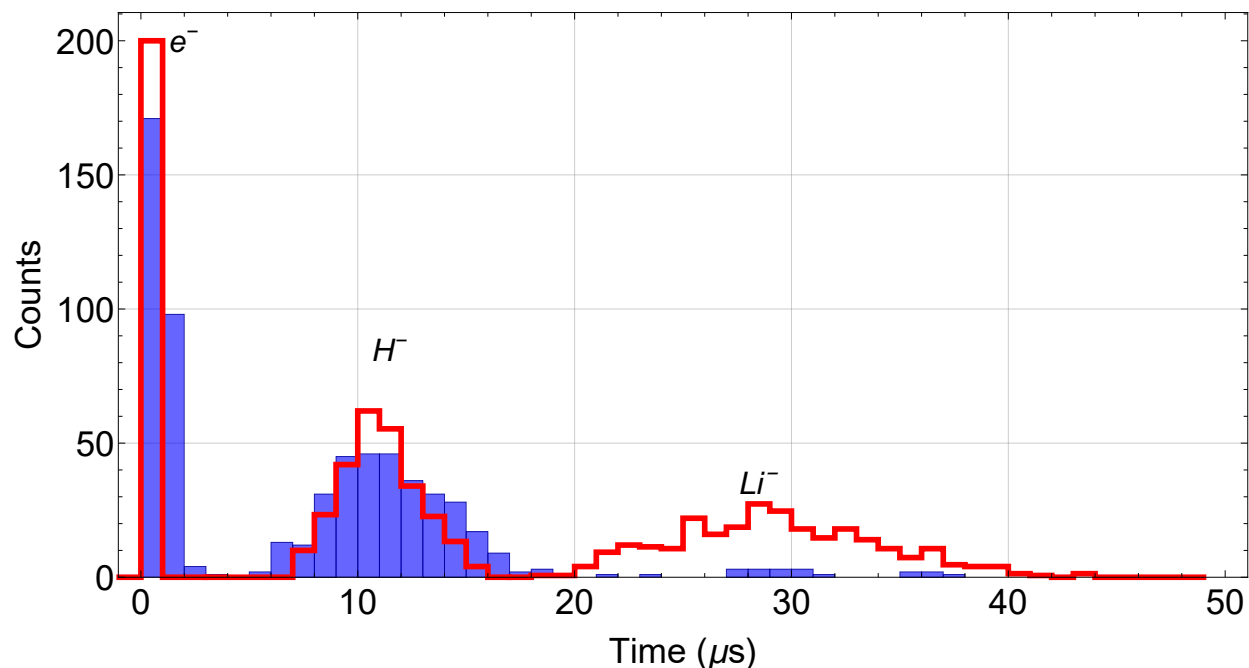


Figure 6. ToF discrimination for negative species showing e^- , H^- and Li^- (or LiH^-) in the same trapping conditions and manipulations as in figure 5 but now doing a quick ramp down from the trap with $E1 = -10$ V, $E2 = -5$ V, $E3 = 0$ V, $E4 = -2$ V to an acceleration ramp with $E1 = -10$ V, $E2 = -5$ V, $E3 = -0.2$ V, $E4 = -0.1$ V and $E5 = 0$ V. The experimental data from an accumulation of 21 runs is shown in blue while a simulated histogram for the species identified is shown with a red envelope. In this figure, $t=0$ is the beginning of the quick ramp down, taken as instantaneous in the simulation. The ablation laser energy was considerably decreased to avoid saturation of the CEM with the e^- signal. See text for more discussion on the “quick ramp down” and Methods for the simulation.

Due to some saturation of the CEM with the electron signal in the ToF, we employed another method to get a ratio of H^- to e^- under these conditions. The electrons arrive at the trap region almost immediately after the ablation in this variation while the H^- 's take about 100 μs. By measuring that the electrons trapped number would not change from 60 to 90 μs, after ablation and before the arrival time of the H^- , we can compare the trapped distribution for slow ramps for samples comprised only of electrons to samples trapped at the best time for H^- . The result is shown in figure 7. The ratio of the areas (~ 3.6) represents that, at its optimal timing, H^- is trapped 2.6 times more efficiently than e^- and with a similar energy distribution.

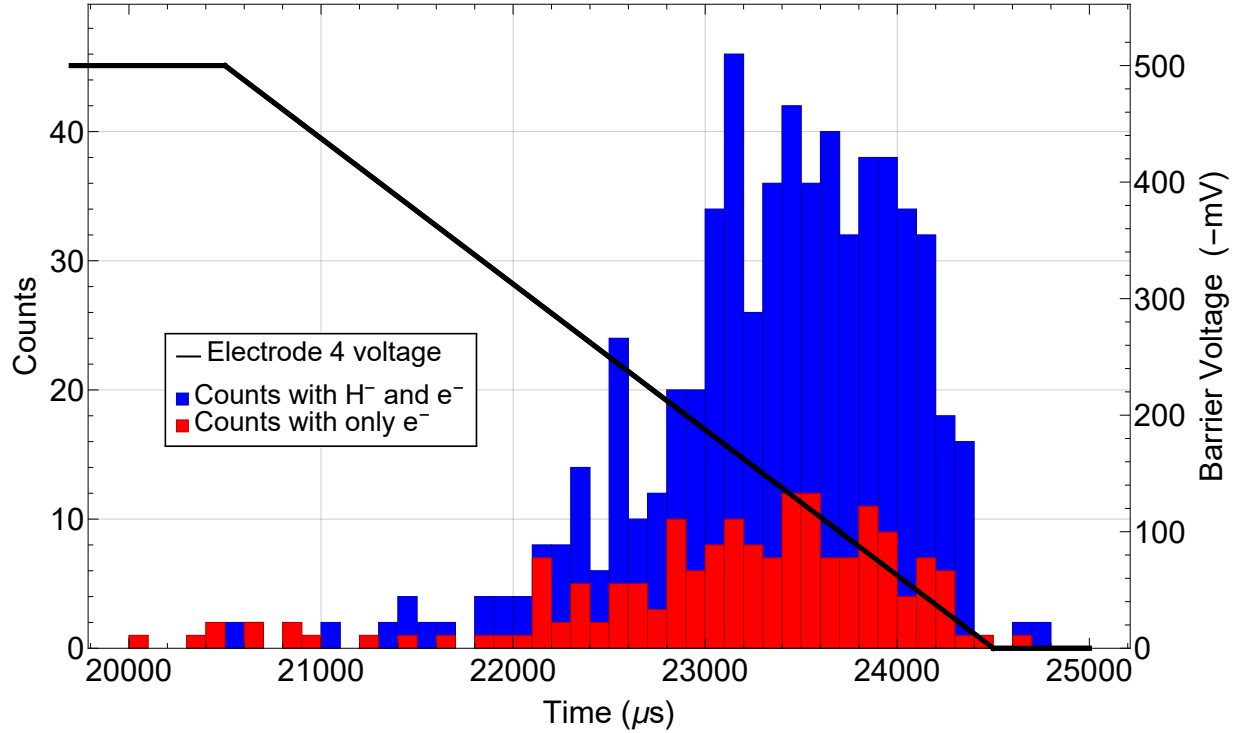


Figure 7. Comparison of slow dumps for a sample trapped at earlier times (60–90 μs after ablation) comprised only of e^- 's (in red), to sample comprised of e^- and H^- (in blue) trapped at the proper H^- trapping time 100 μs after ablation. In these conditions, the ratio of integrated counts results in 2.6 times more H^- 's than e^- 's trapped at the optimized H^- trapping time. The energy distributions are similar.

Another interesting manipulation, able to discriminate masses, is to make the trap unstable to certain species by changing the electrostatic potentials and the magnetic field. For a harmonic Penning trap to be stable³⁹ the cyclotron frequency, $\omega_c = q \frac{B}{m}$, and the axial frequency, $\omega_z \sim 1/\sqrt{m}$, should relate as $\omega_c > \sqrt{2} \omega_z$. The condition relates the confining potential shape (in ω_z), the magnetic field (B) and the particle mass (m) and charge (q). Squeezing and deepening the electrostatic potentials – alternating -10 V and +10 V in electrodes E3, E4 and E5 – we can easily make the trap unstable for species other than e^- and H^- even at the maximum current of 100 A in the trap magnet. Under this quasi-harmonic trap configuration even H^- becomes unstable under ~ 55 A and we performed a study on the trapped particles number as function of the current. Due to a hardware limitation, we could only set the trap magnet current just before sublimation and could not separate the guiding and initial trap loading processes from the trap instabilities. To keep the magnetic field guiding lines configuration unchanged, the sapphire magnet current was changed in the same proportion as the trap magnet current. In figure 8 the result of this study is shown.

The data clearly shows a decrease of the number trapped as the current decreases until a cutoff near 55 A where H^- becomes unstable and the residual counts at lower currents are due to e^- . Two models attempt to capture the qualitative behavior. A first one, in purple, supposes a simple axial 1D model for ions already in a harmonic trap resulting in a step function separating the regions of stability and instability. The other consider the entrance aperture transmission of the

trap, and trap stability also considering the finite electrodes diameters. At the entrance aperture the magnetic field is small, at a ratio of $\sim 1/13$ of that in the trap center, and the radius of curvature of the cyclotron motion may exceed the entrance opening. Inside the trap one may have instability or simply a large cyclotron plus magnetron motion that gets to the electrode walls and lead to losses. Monte-Carlo simulations, using an axial energy distribution like the exponential one in figure 5 inset (despite different conditions and manipulations for this data set to that of figure 5) and different perpendicular energy distribution lead to the other curves in figure 8. The details on the models are presented in Methods.

The good agreement of the last model, without adjustable parameters other than the arbitrary scaling number for the total counts at 100 A, suggests that this method may be further developed as a diagnostic tool for the radial density distribution – requiring validating studies with an imaging detector, or employing an axially displaced photodetachment laser beam, and higher data statistics – or the transverse energy distribution. These are two identified parameters affecting the curves.

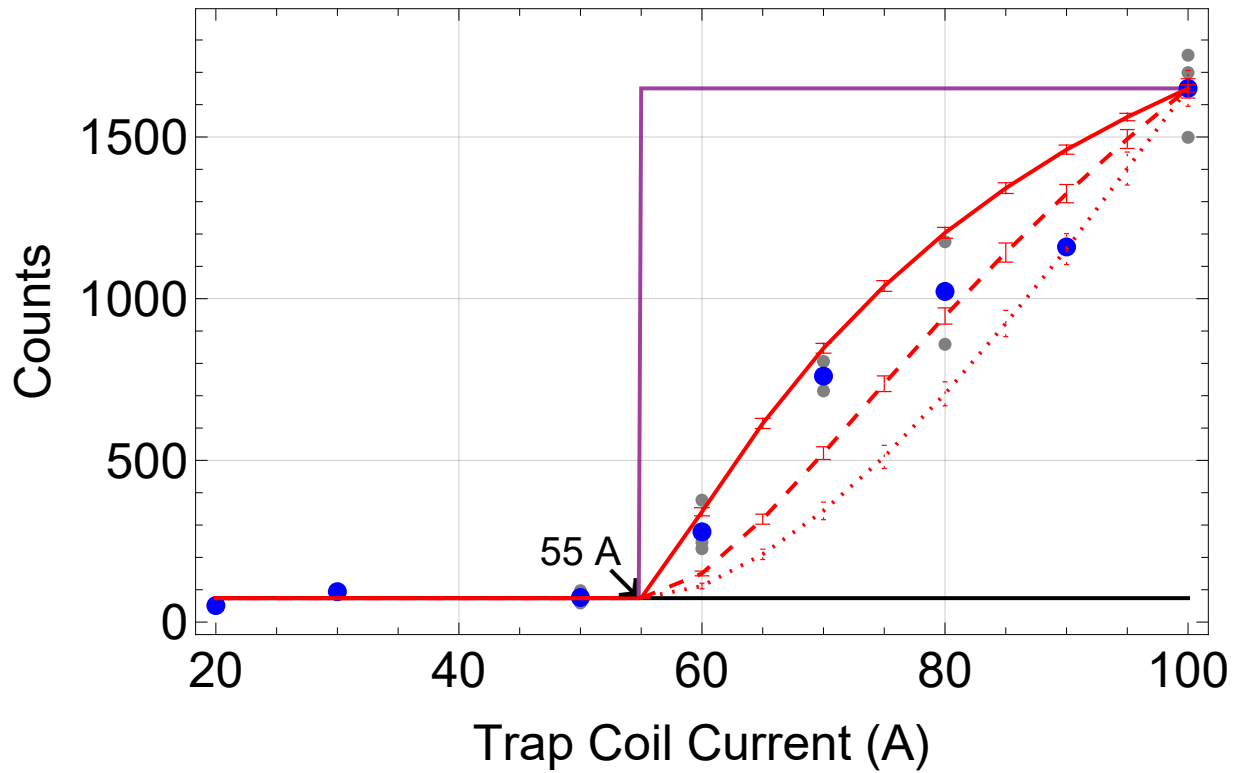


Figure 8. Trap loading and survival of H^- in the trap due to a varying magnetic field. The data is shown as grey dots, representing individual realizations, and the blue dots are the average of the grey dots values for the corresponding current. Two models are shown. The purple line represents a simple axial 1D model concerning only the (harmonic) axial and cyclotron frequencies relation for stability. The red lines guide the eyes through the results of a Monte-Carlo model considering the entrance aperture of trap region, at magnetic fields much lower ($\sim 1/13$) than in the trap, and the survival of the particles in the trap given its diameter for different radial energy distributions. The axial energy distribution is taken as an exponential decay as in figure 5 and the transverse energy distributions are taken as exponential decays but with different energy scales. In the continuous, dashed, and dotted red lines the transverse energy scale is $1/12$, 2, or 20 times the axial energy scale, respectively. Magnetic mirroring effects are taken into effect in the energy rescaling between the trap entrance aperture to the trap center. The models do not include a full particle tracing but only consider the particles at the entrance aperture and the trap center. See text and Methods for further discussion.

The results shown in figures 2–8 above are just a subset of the possibilities with this technique. For instance, we produced trapped H^- from ablation on TiH_2 and performed a few runs with a H_2 , instead of Ne, matrix. In the present trap we can make all atomic masses above 7 (Li), or higher, to be unstable just by squeezing and deepening the potentials, thus making the axial frequency to go over the stability condition compared to the cyclotron frequency. Light particles, like electrons can be expelled from the trap by a fast ($\sim 1 \mu\text{s}$, in the case of e^-) opening–and–closing of the trap barrier, but this required adding some extra complexity to our hardware and software and we performed just a few validating tests. Therefore, one could select a range of masses to keep in the trap for studies such as molecular formation. Splitting the ablation laser, one could simultaneously ablate different targets to produce molecules already in the collision with the sublimating plume or one could press a sintered composite material with the different precursors into a single ablation target. We have also produced a cryogenic beam of electrons from electrostatic sublimation, i.e., we can switch on and off a beam of electrons, and subsequently trap them, just by applying a potential to the sapphire substrate without sublimating a matrix that was previously implanted via laser ablation.

Discussion

In a next generation of the apparatus, with a longer trap magnet – and more uniform field – we will be able to achieve much better mass discrimination and more relevant: stack samples in a very simple manner. Even if we keep only 6 electrodes, we could trap between E0–E3, then move the sample into E3–E5, trap again in E0–E3, then accumulate in E3–E5, and repeat the process. Using a MISu variation we were able to trap over one thousand H^- ’s after a single ablation pulse. With a diode pumped laser operating at high frequency and higher magnetic fields the system can be scaled up by orders of magnitude to large amounts of trapped species. Trapping heavier atomic and molecular ion species at large numbers will also require higher magnetic fields.

This trap holding time was limited by the trap coil’s heating at $\sim 1 \text{ s}$ time scale. In a test, we held a sample up to 1.5 s obtaining ~ 1000 counts in final dump of that realization. In a next realization we plan to use a superconducting coil which, together with a better thermal anchor in the trapping region, should enable long holding times and thus to achieve thermalization and perform evaporative cooling of the trapped samples achieving a few kelvins of temperature.

The system is very rich and has many adjustable parameters that affect the outcome. Despite that, we were able to achieve a robust operation. Moreover, the system still holds many intriguing and open questions. Why we trap only few H^- ’s in the typical MISu procedure. Is the H^- not penetrating the matrix, or being stripped of its extra electron as it enters the solid Ne, or being ionized under the matrix’s high electric fields? Using a variation, we were able to

circumvent the problem and produce large amounts of H^- , but it would be important to better understand this process. We also observed production of these charged species using a H_2 matrix, instead of a Ne matrix, but were not able to do a full exploration on different parameters.

We want to explore the conditions to produce ions at the typical atomic temperatures of kelvins. The MISu technique generates an intense Li beam at a few kelvins, and below, despite Li having a positive (expelling) energy⁴⁰ of 0.25 eV (~ 2900 K) in Ne. This is a strong argument why we expect to produce ions coming from the matrix at these low temperatures as well, even with space charge effects with the ions. The trap closing procedure itself imparts large energy to a fraction of the ions under the rising electrodes potentials and this is clearly seen in figure 3. If these high energy ions would exchange some energy, the “high energy” from our samples could be coming from the dynamic trapping procedure (one gets 1.6 eV average energy from a trap switching to 5 eV, supposing a uniformly distributed flux of ions over the electrodes region). In the contrary direction, the ratio of magnetic fields of 41 mT below the sapphire, where collisions with the Ne gas may not be relevant anymore, to 92 mT in the trap gives some artificial cooling of the measured axial energy since the transverse energy for particles following the field lines will scale with the magnetic field at the expense of the axial energy. We plan to use laser spectroscopy on suitable cations, such as Ca^+ to study the real temperature of the ions’ sample and see in which step of the procedure the sample is gaining energy. At one earlier construction, with different sapphire attaching plates and without all the tools and the trap, we saw time delaying evidence of being able to control and produce a charged sample at speeds comparable to the atomic speeds.

In the present case we still have a large amount of Ne and ions of the opposite charge that come to the direction of the trap. This condition can be mitigated. As for the opposite charges, or stacking, we could easily setup the system with different ablation targets and build a nested Penning trap configuration for positive and negative species trapped side-by-side ready to study molecular recombination, as it is done with $\bar{\text{H}}$ formation by mixing $\bar{\text{p}}$ ’s into a e^+ cloud.

With the electrostatic sublimation of electrons from the matrix, we speculate on producing a low energy spin-polarized beam of electrons. If the matrix is at 3 K and would be subjected to a 4 T field, a spin thermalized electron sample could be 80% polarized. Such a simple low-energy polarized electrons’ source could be very attractive to biochemical experiments, especially with respect to the issue of biology homochirality^{41,42}, and to fundamental quantum collisional processes.⁴³

We believe the data is quite a strong proof-of-principle for what is needed to load H atoms in the \bar{H} ALPHA experiment trap. The system here presented is at a more advanced stage than other alternatives^{44,45} proposed. As for applications with large amounts of ions, such as with tritium or deuterium, we believe the system is scalable. The use of higher power ablation lasers and at high rates, together with higher guiding magnetic fields, would improve the numbers by orders of magnitude.

Conclusions and Prospects

We have demonstrated a platform to produce cryogenic (below 25 meV) beams or trapped samples of electrons, anions, and cations. The system was first designed to produce H^- towards loading the \bar{H} trap in the ALPHA experiment at CERN and we find it meets the necessary criteria of numbers, energy range, and UHV conditions after trapping and waiting the matrix gas to cryopump, for this application. The system should work equally well for T^-/T , perhaps suitable for a neutrino mass experiment, and for D^-/D for studies relevant to fusion research. Trapped anions and cations, or in a beam, can be used to study chemistry at astrophysical conditions, such as in star formation. The system can generate an electrically controlled electron beam which we speculate might be suitable for spin polarization with applications towards studies of chirality with relevance to biochemistry. Based on the present data and previous studies on MISu, the system is quite versatile and general in the sense of being able to produce different species of atomic and molecular neutrals, anions, and cations.

Acknowledgements This work was supported by: CNPq, FAPERJ, and RENAFAP (Brazilian agencies). We thank Profs. Massimo Xi Liu, from USP-São Carlos, and Vitoria Barthelm, from UFRJ, for depositing the NiCr resistive films, first and second batches respectively.

Author Contributions The initial conception was proposed by CLC. All the authors participated in the design and implementation at various stages. LOAA, primarily, and RJSC were responsible for the experimental runs. Data processing was performed by LOAA. The initial manuscript was written by CLC and edited and improved by WW, DMS, RLS, and LOAA.

Reprints and permissions information is available online at www.nature.com/reprints. Readers are welcome to comment on the online version of the paper. Correspondence and requests for materials should be addressed to CLC or LOAA (claudio.cesar@cern.ch , ideazevedo@if.ufrj.br).

Data availability statement The datasets generated during and/or analysed during the current study are available from CLC or LOAA (claudio.cesar@cern.ch , Ideazevedo@if.ufrj.br) on reasonable request.

Competing financial interests The authors declare no competing financial interests.

- ¹ M. Tomza et al., Cold hybrid ion-atom systems, *Rev. Mod. Phys.* **91**, 035001 (2019)
- ² M. Ahmadi, *et al.* Characterization of the 1S-2S transition in antihydrogen, *Nature* **557**, 71 (2018)
- ³ C. J. Baker, *et al.* Precision spectroscopy of the 1S-2S transition in antihydrogen: hyperfine structure and CPT invariance, submitted (2022)
- ⁴ C. L. Cesar, A sensitive detection method for high resolution spectroscopy of trapped antihydrogen, hydrogen and other trapped species, *J. Phys. B* **49**, 074001 (2016)
- ⁵ C. L. Cesar, Trapping and spectroscopy of hydrogen, *Hyp. Interact.* **109**, 293 (1997)
- ⁶ Charman, A. Description and first application of a new technique to measure the gravitational mass of antihydrogen. *Nat Commun* **4**, 1785 (2013)
- ⁷ C. L. Cesar et al., Two-Photon Spectroscopy of Trapped Atomic Hydrogen, *Phys. Rev. Lett.* **77**, 255 (1996)
- ⁸ I. D. Setija et al., Optical cooling of atomic hydrogen in a magnetic trap, *Phys. Rev. Lett.* **70**, 2257 (1993)
- ⁹ K. R. Lykke, K. K. Murray, and W. C. Lineberger, Threshold photodetachment of H-, *Phys. Rev. A* **43**, 6101 (1991)
- ¹⁰ S. Scheidegger et al, Barrier-discharge source of cold hydrogen atoms in supersonic beams: Stark effect in the 1s–2s transition, *J. Phys. B: At. Mol. Opt. Phys.* **55**, 155002 (2022)
- ¹¹ C. Killian, Towards the first demonstration of gravitational quantum states of atoms with a cryogenic hydrogen beam, presentation at the Grasian Workshop, Turku, 2022 (unpublished)
- ¹² O. Amit and T. Udem, Status and plans for the Garching Hydrogen experiments, presentation at the GRASIAN Workshop, Turku, 2022 (unpublished)
- ¹³ S. Vasiliev, H trapping experiments in Turku, presentation at the Grasian Workshop, Turku, 2022 (unpublished)
- ¹⁴ V.V. Nesvizhevsky et al, Quantum states of neutrons in the Earth's gravitational field, *Nature* **415**, 297 (2002)
- ¹⁵ P. Pérez, et al., The GBAR antimatter gravity experiment, *Hyp. Interact.* **233**, 21 (2015)
- ¹⁶ O. Roussele, Quantum interference measurement of the free fall of anti-hydrogen, *Eur. Phys. J. D* **76**, 209 (2022)
- ¹⁷ J. M. Doyle, Energy distribution measurements of magnetically trapped spin polarized atomic hydrogen: evaporative cooling and surface sticking, MIT PhD thesis, 1991 (unpublished)
- ¹⁸ D. M. Asner, R. F. Bradley, et al., Single-Electron Detection and Spectroscopy via Relativistic Cyclotron Radiation, *Phys. Rev. Lett.* **114**, 162501 (2015)
- ¹⁹ J. A. Formaggio, A. L. C. de Gouvêa, R.G. H. Robertson, Direct measurements of neutrino mass, *Phys. Rep.* **914**, 1 (2021)
- ²⁰ M. Bacal and M. Wada, Negative ion source operation with deuterium, *Plasma Sources Sci. Technol.* **29**, 033001 (2020)
- ²¹ A.Dalgarno and R.A.McCRAY, The formation of interstellar molecules from negative ions, *Astrophysical Journal* **181**, 95 (1973)
- ²² A. G. G. M. Tielens, The molecular universe, *Rev. Mod. Phys.* **85**, 1021 (2013)
- ²³ T. J. Millar, C. Walsh, and T. A. Field, Negative Ions in Space, *Chem. Rev.* **117**(3), 1765 (2017)
- ²⁴ S. Robertson, Z. Sternovsky, and B. Walch, Reduction of asymmetry transport in the annular Penning trap, *Phys. Plasmas* **11**, 1753 (2004)
- ²⁵ D. Faircloth and S. Lawrie, An overview of negative hydrogen ion sources for accelerators, *New J. Phys.* **20**, 025007 (2018)
- ²⁶ Feldker, T., Fürst, H., Hirzler, H. et al. Buffer gas cooling of a trapped ion to the quantum regime. *Nat. Phys.* **16**, 413–416 (2020)
- ²⁷ T. Yang, et al., Isomer-specific kinetics of the C + H₂O reaction at the temperature of interstellar clouds, *Sci. Adv.* **7**, 1 (2021)
- ²⁸ D. J. Wineland and H. G. Dehmelt, Principles of the stored ion calorimeter, *J. Appl. Phys.* **46**, 919 (1975)

- ²⁹ F. Diedrich, J. C. Bergquist, W. M. Itano, and D. J. Wineland, Laser Cooling to the Zero-Point Energy of Motion, *Phys. Rev. Lett.* **62**, 403 (1989)
- ³⁰ M. Bohman et al., Sympathetic cooling of a trapped proton mediated by an LC circuit, *Nature* **596**, 514 (2021)
- ³¹ J. Eschner et al., Laser cooling of trapped ions, *J. Opt. Soc. Am. B* **20**, 1003 (2003)
- ³² P. Yzombard, et al., Laser Cooling of Molecular Anions, *Phys. Rev. Lett.* **114**, 213001 (2015)
- ³³ G. B. Andresen, *et al.*, Evaporative cooling of antiprotons to cryogenic temperatures, *Phys. Rev. Lett.* **105**, 013003 (2010)
- ³⁴ R. Lambo, C. C. Rodegheri, et al., Spectroscopy of low-energy atoms released from solid noble-gas matrix: Proposal for a trap loading technique, *Phys. Rev. A* **76**, 061401(R)
- ³⁵ R. L. Sacramento, et al., Source of slow lithium atoms from Ne or H₂ matrix isolation sublimation, *J. Chem. Phys.* **136**, 154202 (2012)
- ³⁶ R. L. Sacramento, et al., Matrix Isolation Sublimation: an apparatus for producing cryogenic beams of atoms and molecules, *Rev. Sci. Instrum.* **86**, 073109 (2015)
- ³⁷ A. N. Oliveira, et al., Heteronuclear molecules from matrix isolation sublimation and atomic diffusion, *J. Chem. Phys.* **149**, 084201 (2018)
- ³⁸ W. C. Wiley and I. H. McLaren, Time-of-Flight Mass Spectrometer with Improved Resolution, *Rev. Sci. Instrum.* **26**, 1150 (1955)
- ³⁹ G. Werth, V.N. Gheorghe, F.G. Major, *Charged Particle Traps II*, Springer Series on Atomic, Optical, and Plasma Physics **54** (2009)
- ⁴⁰ M. E. Fajardo, Matrix isolation spectroscopy of metal atoms generated by laser ablation. II. The Li/Ne, Li/D₂, and Li/H₂ systems, *J. Chem. Phys.* **98**, 110 (1993)
- ⁴¹ S. Mayer and J. Kessler, Experimental Verification of Electron Optic Dichroism, *Phys. Rev. Lett.* **74**, 4803 (1995)
- ⁴² M. Kettner, V. V. Maslyuk, D. Nürenberg, et al., Chirality-Dependent Electron Spin Filtering by Molecular Monolayers of Helicenes, *J. Phys. Chem. Lett.* **9**, 2025 (2018)
- ⁴³ M. Dapor, Polarized electron beams elastically scattered by atoms as a tool for testing fundamental predictions of quantum mechanics, *Sci. Reports* **8**, 5370 (2018)
- ⁴⁴ S. A. Jones, An ion trap source of cold atomic hydrogen via photodissociation of the BaH⁺ molecular ion, *New J. Phys.* **24**, 023016 (2022)
- ⁴⁵ W. A. Bertsche et al., A low energy H⁻ beamline for the ALPHA antihydrogen experiment, *J. Phys.: Conf. Ser.* **2244**, 012080 (2022)

Methods / Supplementary Material:

Time-of-Flight mass discrimination (ToF-MD) of trapped species

Once the ions are trapped, we have implemented a potential ramp to discriminate the masses. A Wiley-McLaren³⁸ configuration would require a free-flight region twice as long as the accelerating region. Within our trap space constrain, we could switch from a trap configuration with potentials (in V) $E_2 = 5, E_3 = 0, E_4 = 1$ and $E_5 = 0$ to the configuration of $E_2 = 5, E_3 = 0.2, E_4 = 0.1$ and $E_5 = 0$ (or $E_2 = 5, E_3 = 0.4, E_4 = 0.2$ and $E_5 = 0$) as shown in figure 8 below.

For initial estimates of this ToF-MD functionality we used a simple analytical function that approximately simulate each electrode potential and added their values to represent different trap configurations. The simplest function, with just 3 adjustable parameters, is given by:

$$V(z) = \sum_{n=0}^5 f_A A_n \left\{ \text{Erf} \left(\frac{dz + (z - z_{0n})}{\delta z} \right) + \text{Erf} \left(\frac{dz - (z - z_{0n})}{\delta z} \right) \right\},$$

where A_n, z_{0n} represent the applied voltage amplitude and the center position of the n^{th} electrode. The geometrical factor $f_A \approx 0.47$, $\delta z \approx 7$ mm, and $dz \approx 11$ mm is the length of the electrode (10 mm) plus the distance between electrodes (1 mm). From the above expression the electric field can be analytically obtained.

The configuration for the ToF-MD, with precise potentials, is shown in figure 9 below. Notice that the electric field is not ideally uniform in the acceleration region but shows wiggling, and the free-flight region is small compared to the acceleration one.

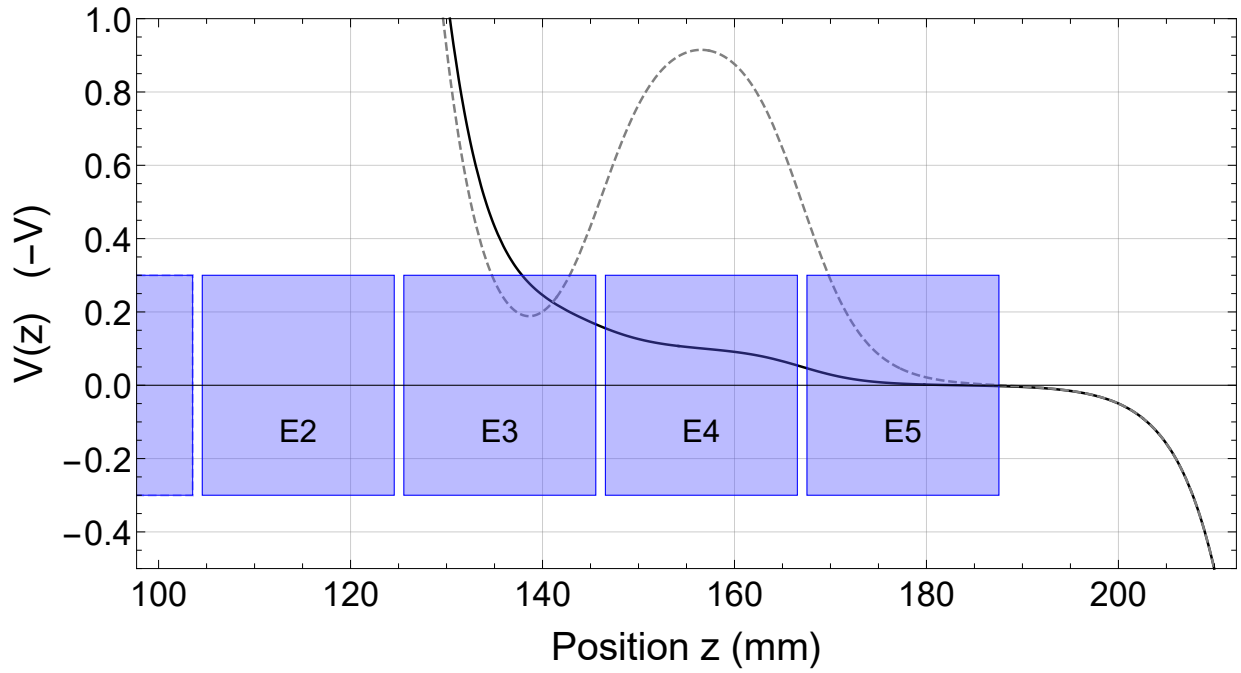


Figure 9. ToF mass discrimination potentials (depicted for the case of anions). The dashed curve is the initial trap around E3 ($E_2=5$ V, $E_3=0$, $E_4=1$ V, $E_5=0$) before the potentials are switched to the ToF configuration ($E_2=5$ V, $E_3=0.2$ V, $E_4=0.1$ V, $E_5=0$) shown in solid line. The negative potential at $z > 200$ mm is due to the CEM.

The simulation considered a 1D system, along the trap axes, concerning only the electrostatic field produced by the electrodes and CEM detector and not the magnetic field. According to the energy distribution in figure 6, we place ions at the returning points in the trap, in both ends, given its energy and let each ion evolve inside the trap for a random time between 0 and half of the period of axial oscillation for that energy. This new state of each ion is the corresponding initial state for the second part of the simulation where the trap is switched instantaneously to the ToF configuration. The actual driving hardware takes about $1.2 \mu\text{s}$ to reach 90% of the set value and this would cause extra spreading in the detection time distribution, but it was not considered in the simulation. The results are sufficient for discriminating our species of interest for this work.

For the ToF-MD simulations shown in figure 6 we used an interpolation for the electrodes' voltage configuration, $V_{ToF-MD}(z)$, given by a finite element package solver instead of the analytical potential described above. The time-of-flight is given by the usual integration $t_{ToF-MD} = \int_{z_0}^{z_f} \frac{1}{\sqrt{\frac{2}{m}\{\epsilon - q V_{ToF-MD}(z)\}}} dz$, where z_0 is the position at the time of switch, z_f is a position near the

CEM – where particles at rest would take less than 0.2 μs to reach the CEM – and ϵ is the total energy the particle has immediately after the switch, i.e., its initial kinetic energy (when it was in the trap) plus the potential energy in ToF configuration: $q V_{ToF-MD}(z_0)$.

Magnetic field variation study

To analyze the stability of H^- and the losses by collisions in the trap entrance as we change the trapping/guiding magnetic field, we repeated for different magnetic field conditions the following steps: a matrix of about ~ 370 nm is grown; the currents on the magnets are set to the desired value (at maximum, 100 A in the trap magnet and 2.5 A in the sapphire coil); during a slow sublimation, a single laser ablation hits the LiH target; the trap loading potential, with the electrode configuration (in V) $E_0=0, E_1=0, E_2=-5, E_3=0, E_4=0, E_5=-5$, is closed 100 μs after the ablation; the sample is adiabatically squeezed by changing the electrodes configuration (in V) to $E_0=0, E_1=0, E_2=0, E_3=-10, E_4=10, E_5=-10$ and waiting for 1 ms; particles with energies above ~ 700 meV are released by changing the electrode configuration (in V) to $E_0=0, E_1=0, E_2=0, E_3=-10, E_4=0, E_5=-1$; after 500 μs the remaining trapped particles are slowly released and detected. The data is shown in figure 8.

Some assumptions were made for constructing the models (1D and 3D) to qualitatively describe the survival of H^- after this process. A uniform magnetic field along all the trap volume was considered, as the trap is just one electrode wide, taking the mean value of field in the region. We considered the trap to be harmonic for energies < 700 meV since the axial oscillation frequency changes less than 2% within this energy range, hence the equations for the stability inside the trap are exact. The simple axial 1D model only considered the stability criteria of the relation of the cyclotron and axial frequencies. For the 3D models, we considered an axial (z) exponential decaying energy distribution as measured in Figure 5. The transverse energy distribution was also considered exponential but with different decay values and it was initially mapped only on v_y . The initial position of the anions in the xy-plane inside the trap (x_0) imitates a uniform surface distribution but mapped only in x with probability proportional to x .

The axial and transverse energies are drawn for a particle inside the trap. Considering the transverse energy adiabatic propagation in magnetic field – where the transverse energy scales with magnetic field at the expense of axial energy – we map both the transverse and axial energies to the entrance ($\epsilon_{t,in}$ and $\epsilon_{z,in}$) of the trap region (just left of E_0). If $\frac{\epsilon_{z,in}}{\epsilon_{t,in}} > \frac{B_{trap}}{B_{in}} \approx 12.85$, where B_{trap} and B_{in} are the magnetic fields at the trap and at the entrance, the particle

is considered in the Monte-Carlo since it will not reflect magnetically. If $\epsilon_{t,\text{in}} > 172$ meV the cyclotron radius is greater than the entrance radius and we consider the particle lost at the entrance. If the particle enters the trap, given the drawn initial position (x_0) and transverse energy inside the trap ($\epsilon_{t,\text{trap}}$, supposed initially along y), we calculate the maximum radius⁴⁶ of the particle as the sum of the magnetron and cyclotron radii for this particle for each current considered. If this maximum radius, for each current, is larger than the electrode radius this particle is lost in the trap. Finally, if the current is below ~ 55 A, the trap is unstable and no H^- would be trapped.

The shapes of the curves resulting from these simulations have a dependence with the transverse energy distribution (see Figure 8). Figure 10 shows the histograms of distributions for the particles that survived the losses considered for the trap at 100 A consisting of the transverse and axial energies ($\epsilon_{t,\text{trap}}$ and $\epsilon_{z,\text{trap}}$) distributions and initial position (x_0) considering three different initial distributions for the transverse energy.

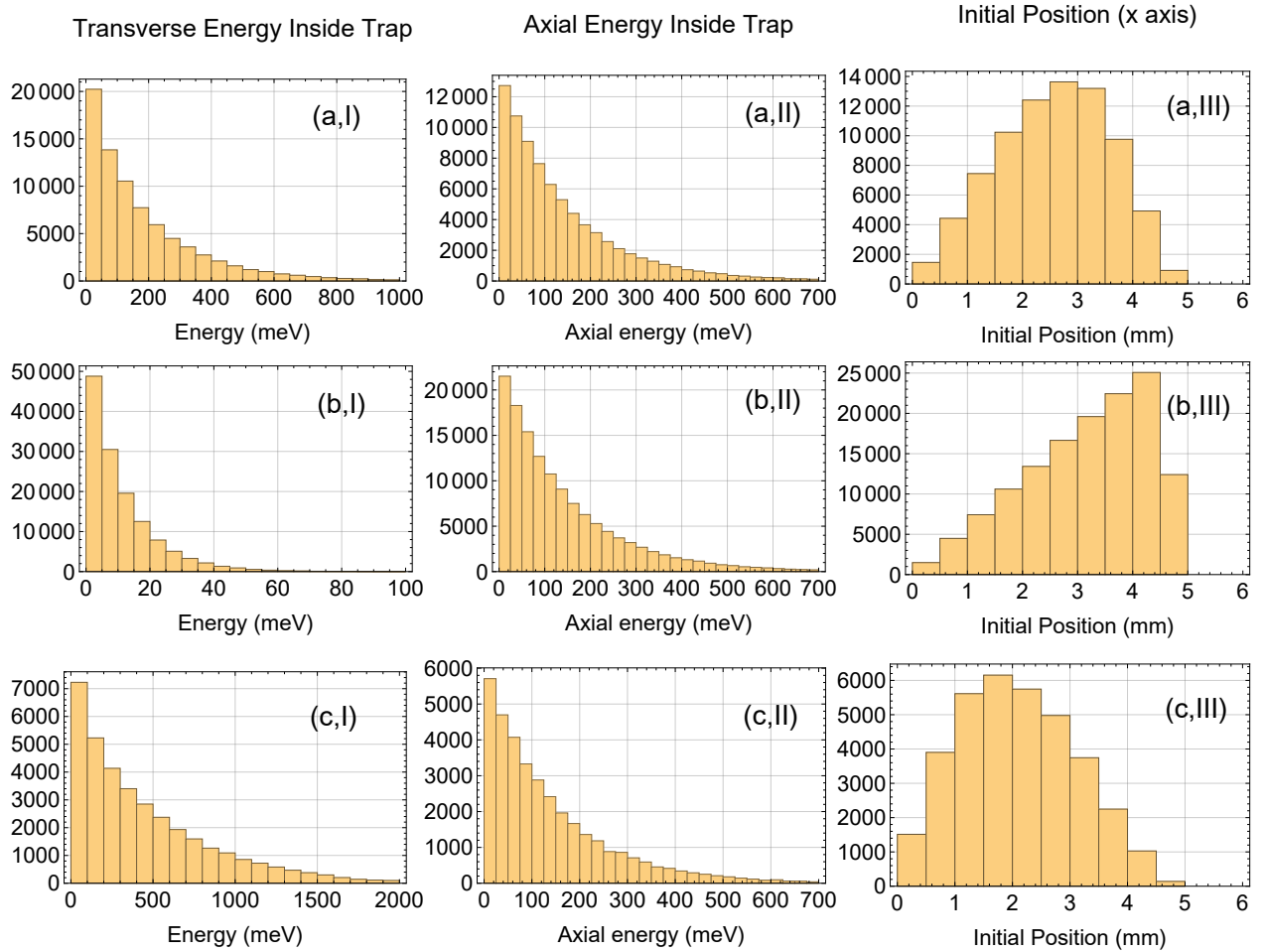


Figure 10. Histograms from the Monte-Carlo Simulations of the surviving particles inside the trap for a trap coil current of 100 A for the 3D model with different exponential energy scales for the transverse energy distribution: (a) 2 times greater than in the axial distribution, (b) 12 times smaller and (c) 20 times greater. In all three cases an exponential decaying axial energy distribution was assumed in the beginning, but some low energy particles are magnetically reflected and thus considered not trapped. Notice

the very large loss at the highest transverse energy distribution from the total of 150000 particles, simulated at each case. See text for discussion.

⁴⁶ M Kretzschmar, Particle motion in a Penning trap, *Eur. J. Phys.* **12** 240 (1991)